Chapter 19

Stability assessment in advanced DC microgrids

Daniele Bosich[1], *Massimiliano Chiandone*[1] *and Giorgio Sulligoi*[1]

The DC technology appears as promising in enabling new advanced microgrids. The reason is to be sought in the distributed implementation of PV renewable energy sources and battery storage systems, which actually operate by a DC distribution. When a widespread use of power converters guarantees the DC microgrids functionality, an attentive evaluation is to be carried out on the DC stability matter. The present chapter wants to investigate the methods to assess the stability in isolated DC distribution systems. As the latter can be lost when high are the converters control bandwidths, analytical developments are proposed to correlate requested control performance and poles positioning. If the methodology is initially conceived for a classical DC radial distribution, a final study will transfer it on complex DC Zonal Electrical Distribution Systems.

19.1 Introduction

In recent years, the impressive advancements in power electronics have launched the DC technology as decisive in the modernization of electrical power distribution. Indeed, nowadays the latter not only has to guarantee the proper loads supply, but also it has to ensure the requirements of efficiency and sustainability. Only the smart implementation of a totally controlled grid can be the answer when pursuing these upgraded features. As a matter of fact, the two requirements are now fundamental to get the transition in electric power generation towards the green era. The desired transformation in the way of managing the energy is mainly supported by the adoption of Distributed Energy Resources (DER) and storage. The available technologies for DER (e.g. photovoltaic plants, wind farms, hydropower plants, etc.) and storage (e.g. batteries, pumped-hydro plants, flywheels, etc.) are revolutionizing the concept of electrical distribution grid into the new one of controlled microgrid. Thanks to the wide utilization of power conversion, the latter is able to address the power flows in real time, while at the same time fostering the exploitation of aleatory sources

[1]Department of Engineering and Architecture, University of Trieste, Italy

thanks to the storage. Although the microgrid concept has been conceived for the low-voltage AC grids [1], the adoption of the DC technology appears now feasible and effective for the microgrids implementation [2–4]. Not only the DC distribution can promote the sustainability in the residential context [5,6], but other important benefits can make the DC microgrids convenient when feeding the onboard users of electric ships [7–12]. In land applications, the DC microgrids are well regarded being simplified the integration of DC subsystems, like PV generation and battery storage. Differently, in shipboard context the direct current can play an important role when chasing the space-weights reduction in power systems [13,14]. Indeed, when adopting the DC technology to reduce the space for hosting the electrical installations, new onboard areas are made available to increase the ship pay-load [15,16]. If on one side the DC distribution is powerful to increase the system flexibility (with all the related advantages), on the other such a feature is made possible thanks to a widespread use of controlled power converters. In a DC distribution, the latter are responsible to interface sources-loads to the DC bus (i.e. radial distribution [13]) or to interconnect a specific source-load area (i.e. zonal distribution [17]). Whatever the distribution is implemented, a large use of controlled power converters is undeniable for enabling a smarter management of sources and loads. Evidently, each converter must be equipped with a proper filtering stage to ensure the power quality requirements on DC distribution [13]. On the other hand, a not optimized match between controlled converter and filter can induce voltage oscillations and even the instability if the DC grid is isolated. By considering the importance of system stability [18], the present chapter wants to investigate on the destabilizing phenomena in advanced DC microgrids. First, Section 19.2 provides the basis for modeling islanded DC distributions, with a particular attention on simplifying assumptions (i.e. Constant Power Load (CPL) or controlled load's model) and system topologies (i.e. radial and zonal). After an introduction on the possible destabilizing resonance in DC grid, great importance is put on the control systems, which actually can be responsible for the instability in bad-designed filtered systems. Once defined the scenario, Section 19.3 is conversely oriented on the methodology to assess the DC stability. By starting from the mathematical models of DC controlled systems, a convenient procedure is proposed to finally find the system poles, thus verifying the stability requirement. Finally, Section 19.4 shows an example where the proposed methodology is able to predict the DC grid's behavior.

19.2 DC power systems modeling

The future power distribution will be based on a large employment of electronics converters to proficiently address the power flow, while at the same time ensuring controllability, flexibility and sustainability, both in land and in marine applications [4, 10]. Among the different distributions, the one based on DC appears to be a convenient possibility, especially when integrating subsystems naturally operating in DC current (i.e. PV, storage). When the DC technology is adopted to distribute the power towards the loads, unstable behaviors can occur when the LC filtering arrangements are not properly tuned on the DC–DC converters' control bandwidths. This phenomenon is

made evident in an isolated DC microgrid feeding a high-performance controlled load. In such a case, a perturbation on the bus (i.e. load connection) can potentially trigger the system instability, thus the protections intervention. If the DC microgrid operates in islanded configuration, the blackout results consequent as well as the negative outcomes related to microgrid switch-off. During the last 25 years, a great effort has been spent in analyzing this destabilizing resonance, firstly assuming the condition of infinite bandwidth on the load converter control, thus the so-called CPL model [19–22]. Although this nonlinear representation does not constitute the worst case scenario [23], a large bibliography has been developed on the control systems to compensate for the CPL instability. Not only several contributions have considered the CPL infinite bandwidth's assumption in the near past [24–28], but also nowadays the same hypothesis is conventionally adopted to synthesize the stabilizing control in DC microgrids [29–33]. In the cases discussed in bibliography, the CPL modeling results convenient for two main reasons: on the one hand, it is representative of a well-recognized critical case (i.e. small/negative damping factor when a filtered DC–DC converter feeds a CPL), on the other hand, the no-dynamics modeling of a CPL is simple and straightforward. A different approach has been proposed by the authors to overcome the nonlinear CPL modeling, then investigating in detail the reason of DC system instability. Particularly, the works [34–37] have demonstrated how the unstable behavior is strictly related to the control performance on load converter. In other words, the infinite bandwidth of CPL is now made finite, where its magnitude greatly influences the stability behavior for a given LC filter on the DC load. A not integrated and consequential design of filtering stage (i.e. resonance frequency ω_f) and control (i.e. bandwidth ω_c) is the cause of DC instability, as observed in the optimization process in [38].

From this background, this section discusses about two islanded DC distributions on which study the system stability in the presence of perturbations. As seen before, the applied perturbation (e.g. load step, generating converter disconnection, etc.) can provoke unstable behavior on the DC filtered system in the presence of large controlled bandwidths on the loads side. Therefore, the models to represent the DC distributions must enable the possibility to manage/change the control bandwidths on controlled DC–DC converters. To do this, evidently the CPL assumption is overtaken, whereas the simplified modeling in [34–37] constitute the effective way to take into account the load converter dynamics and its effect on stability. In this regard, detailed considerations on the microgrid controls are in Section 19.2.3. For what concerns the possible DC distributions, the authors have concentrated their attention on the marine context. This particular scenario is noteworthy when discussing about the DC stability. Indeed, the complex DC shipboard grids are designed to supply large power (MW) to the loads, the LC filters are possibly downsized for space reasons while the system is islanded by definition [7,10,39]. All the three features make the shipboard DC microgrid a challenging test-bed on which assessing the system stability. In this chapter, the two electrical distributions on which evaluate the destabilizing effects are therefore collected from the IEEE Standard 1709 [13]. Such a standard is of paramount importance, as it provides a precise overview on controlled Medium Voltage DC (MVDC) power systems on ships. Although this standard is therefore focused on the marine applications, most of the guidelines are anyway transferable to a generic DC

microgrid. Thus, the methodology to assess the stability is first conceived on complex MVDC shipboard grids. Later it can be applied on controlled Low Voltage DC–Medium Voltage DC (LVDC–MVDC) distribution systems to establish the stability performance in islanded microgrids on land.

19.2.1 Radial distribution

The system stability is firstly evaluated on the DC distribution proposed in Figure 19.1. In this radial topology [13], the generating part is depicted on the left, while the controlled loads are on the right. The system is supposed to be powered by a Diesel engine and a gas turbine, then the buffering function is guaranteed by a dedicated storage system (e.g. capacitor bank, batteries, fuel cells). Also, a shore connection platform on the right can feed the DC onboard system when the ship is mooring at the port. Clearly, several components are necessary to make available the generating/stored power. The cascade of AC generator (i.e. synchronous machine) and generic AC–DC rectifier is employed to make available the power from diesel/gas prime movers. The same power conversion's solution also for exploiting the landed power from the shore connection [40–42]. Each AC–DC interface can be uncontrolled or controlled. In the first case, a standard 6-pulses diodes bridge is able to impose an unregulated DC voltage, whose average value is proportional to the AC line–line Root Mean Square (RMS) voltage at the interface input (i.e. 1.35 is the ratio). Conversely, in the second case, Insulated Gate Bipolar Transistor (IGBT) switches are used to implement a totally controlled Active Front End converter to regulate voltage/current at the output of AC–DC power conversion stage. When the AC–DC power conversion is uncontrolled, an additional DC–DC buck-boost converter is conventionally added at the diode rectifier output to control the DC bus voltage. Differently, such a stage is not necessary if the AC–DC stage is able to regulate its voltage/current outputs. Other DC–DC interface is finally used to enable the charge/discharge functionality on battery modules. For what regards the power scheme on the right, several DC–DC converters work as interfaces towards the onboard loads. As the standard is focused on marine shipboard systems, also the loads are typical of the marine context. Thus, it is possible to enumerate the drives for moving the ship propellers, high-demanding loads such as the radar and the pulsed one and finally generic ship service load centers. Evidently, the widespread utilization of power converters on the one hand increases the flexibility in managing the onboard power toward the loads, on the other hand, enables high-performing dynamics performance on controlled loads. A similar complexity in electronics interfaces is also expectable in terrestrial DC microgrids working in islanded mode, where conversely the power conversion is mainly devoted in ensuring the optimization in power management, then pursuing the target of sustainability.

19.2.2 Zonal distribution

The distribution in Figure 19.2 is the zonal case where assessing the DC system stability. This innovative structure is envisaged in the IEEE Std 1709 [13], where the so-called Zonal Electrical Distribution System (ZEDS) is proposed as a flexibility

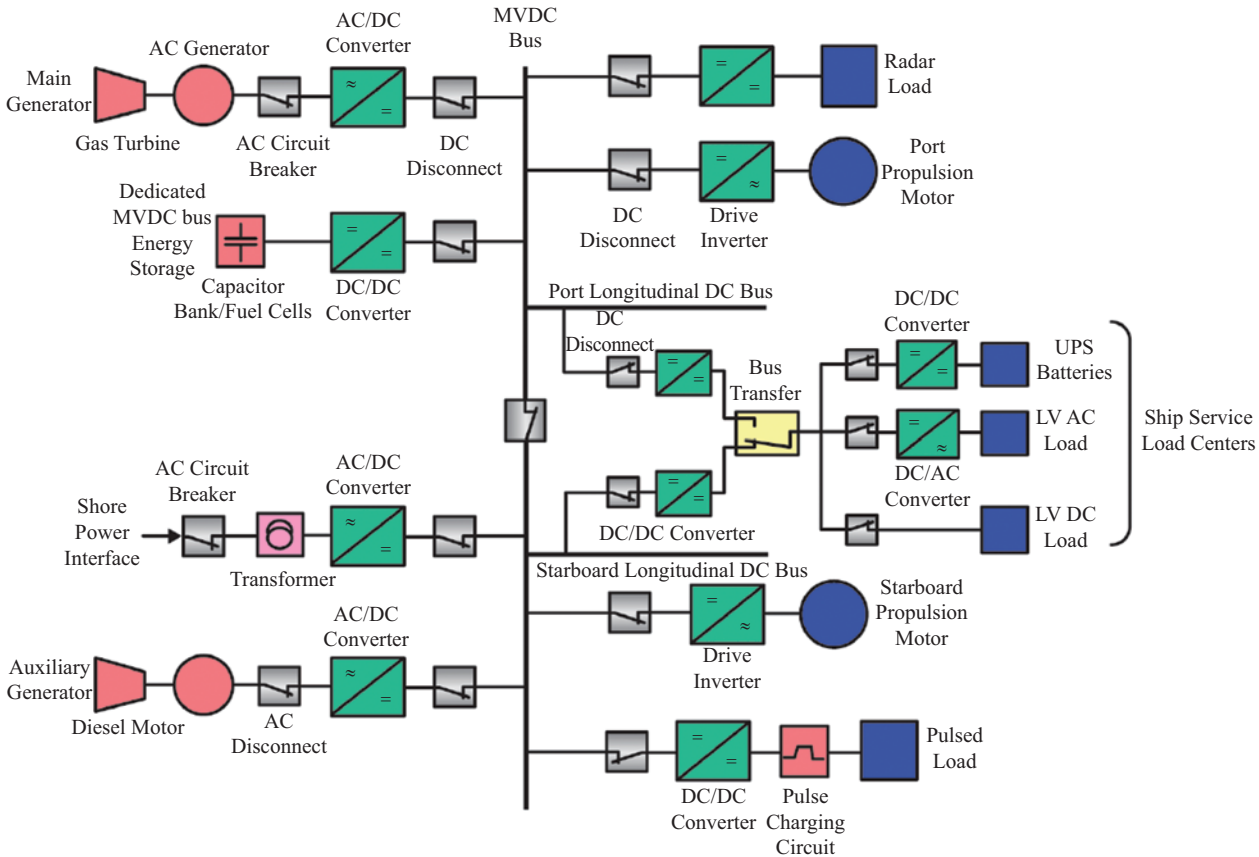

Figure 19.1 Radial DC marine power system [14]

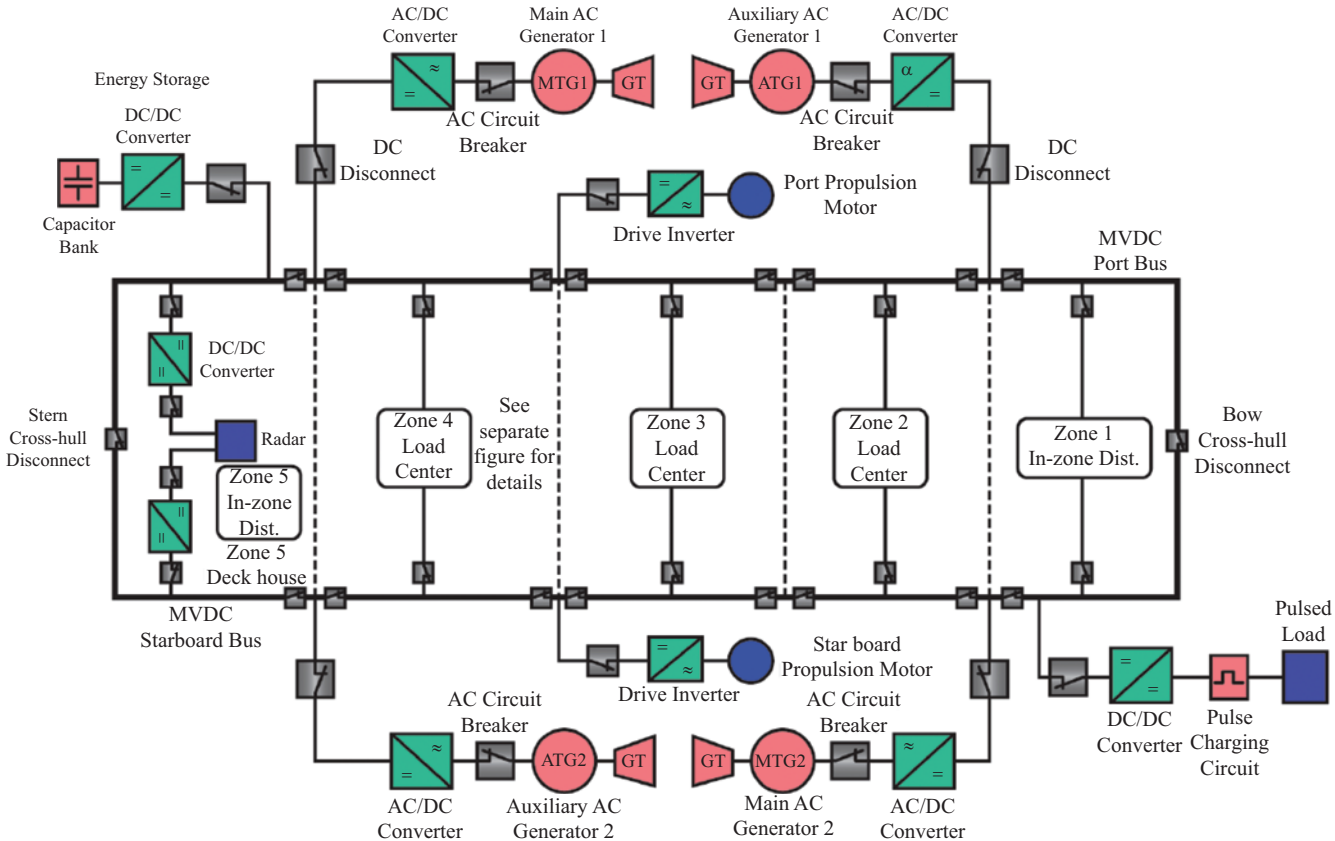

Figure 19.2 Zonal DC marine power system [14]

enabler for marine applications. The ZEDS topic is introduced in the IEEE Std 1826 [17], which identifies the zonal distribution as logical transition from the previous concepts and guidelines introduced in the IEEE Std 1662 [43] and the IEEE Std 1676 [44]. In this regard, the IEEE Std 1826 introduces the ZEDS as a power electronics open system interface with a power rated above 100 kW. Albeit the ZEDS topic has been proposed for navy shipboard power systems since 20 years [45], a recent contribution [46] has clarified the control systems and protections as they are essential in the management of such an islanded flexible grid. In such a zonal system, the ZEDS is configured to feed a group of loads as conceived in [17]. Particularly, ZEDS and its supplied loads are part of a larger set called Zone. This corresponds to the smallest logical-physical grouping of generating units, storage systems, and consumption (Figure 19.2). By means of a limited number of power/control interfaces, one or more external power systems (or other Zones) are interconnected to each Zone. The potentiality in reconfiguring each Zone appears evident and summarized in its intrinsic features: (a) it contains one or more independent power device, (b) it operates as an integral part of a larger system (normal operation), (c) it is capable of working independently for a short time (special operating conditions). As in [17,45–48], the ZEDS plays the role of linking block among the several grids, while showing some characteristics that are fundamentals in the marine case (i.e. redundancy, reconfigurability, fault resilience, and high efficiency). Such important advantages are guaranteed in the presence of a smart control system [49–51], which is designed and optimized to implement the master–slave strategy (i.e. centralized control), the independent/communicating controls and intelligent devices (i.e. distributed control), or the global control without communication (i.e. autonomous).

The ZEDS hierarchical control architecture is shown in Figure 19.3, where the function layers are depicted. To give a complete treatise about this architecture [17,46], in the following, the main functions are presented: (1) the external-to-bus conversion block to manage the power flow between in/out of a ZEDS; (2) the in-zone distribution bus to similarly ensure the power exchange among the ZEDS subsystems; (3) the in-zone energy storage system to guarantee the PQ/QoS requirements; (4) the in-zone generation element to support the power production inside the ZEDS; (5) the bus-to-internal conversion element to properly adapt the output supply; (6) the faults prevention in the the conversion system; (7) the distribution panel to interface the final devices. All the elements here described are connected through power electronics interfaces to avoid interruption in power supply during the transition from one interface to the next one. To ensure this functionality, three control functional layers are adopted: (a) multi-zone control (time constant above 100 ms) to coordinate the system mission/duties; (b) zonal control (time constant above 10 ms) to manage the in-zone control in order to impose the zone mission; (c) in-zone control (time constant smaller than 10 ms) to regulate the actions of power electronics components. Once the time constants are defined in Figure 19.3, the first-order assumption on the controls is useful to easily find the control bandwidths, then consequently provide guidelines for getting the dynamics decoupling in ZEDS controls. Then, by mathematically inverting the time constants, the consequent control bandwidths are found as 10–100–1000 rad/s. The decoupling is an important requirement to be attained when designing

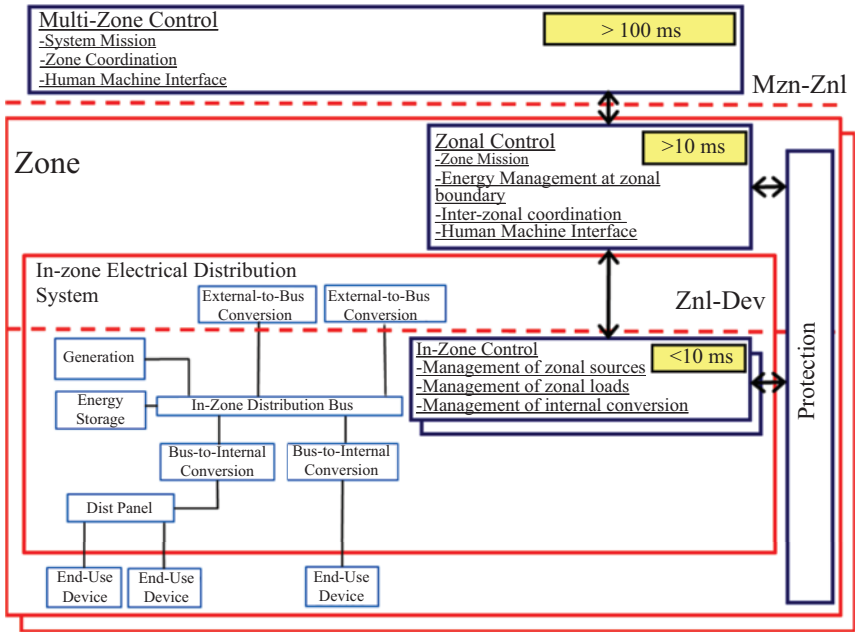

Figure 19.3 ZEDS hierarchical control architecture [46]

the control loops. To prevent destabilizing interactions among controls, a convenient repositioning [46] in accordance to the IEEE Std 1826 [17] configure three increasing bandwidths, where the one decade distance is imposed. The bandwidth on multi-zone control bandwidth is put equal to 5 rad/s. The zonal and in-zone bandwidths are, respectively, 50 and 500 rad/s.

19.2.3 DC voltage control

Both in radial (Figure 19.1) and in zonal (Figure 19.2) distributions, the DC–DC interface converters are the actuators to guarantee the system operation on stable equilibrium points. As in [52], three are the main control strategies (i.e. centralized, decentralized, and distributed) to properly manage the power electronics in DC microgrids. In general, the interfaces based on power electronics support the chosen strategy by performing the current or the voltage controls as output targets [53,54]. In the first case, a PI current loop is used to regulate the operation of a DC–DC interface converter (i.e. buck, boost, buck-boost topology). Such an action is aimed at imposing a certain current (i.e. reference) at the converter output. Differently, the PI voltage control on DC–DC converter (again step-up or step-down system) wants to calibrate the duty cycle to ensure the desired voltage at the converter output stage. As the voltage-controlled converters force the energization on DC grid, their importance results apparent. In a DC distribution with several interfaces, some DC–DC converters are usually current-controlled while the others are in charge of imposing the reference DC voltage on the bus. As multiple converters govern the same bus

voltage, thus droop functionality is mandatory to ensure a bus voltage near the rated value (i.e. small droop coefficients) while sharing the power among voltage-controlled converters [10]. Hierarchical control strategies for DC systems are in [55–57].

19.3 Methodology to assess the DC stability

This section wants to propose a new methodology to investigate the stability in islanded DC microgrids, like the ones adopted in marine applications. As these power systems are isolated from the infinite-power point (e.g. the PCC, Point of Common Coupling), the system stability can be easily put in danger. The absence of this fundamental requirement means uncontrolled voltage oscillations in the presence of perturbations (i.e. load reconfigurations), definitely the protections interventions and the system blackout. The stability relevance is even more evident in the DC controlled grids where destabilizing resonances can be more common especially when control and LC filters arrangements are not conscientiously tuned in a stability-oriented system design [38]. In this regard, the authors have proposed a complete study on DC stability assessment in [58]. This paper follows a first research interest, where pursuing the definition of an aggregated method to understand how multiple-differently controlled converters impact on the system stability of a DC radial grid. By posing on important assumptions and initial hypotheses, this important work proposes a method to largely simplify the stability analysis while ensuring the analytical study even when the controlled loads are numerous. Different research trend the one followed in this section, where conversely the system complexity is maintained and the poles definition is achieved by digital tools. To gets the numerical evaluation on DC stability performance, a multi-model methodology is here proposed as in [53]. This advanced method is based on the determination of several subsequent models. Their development is actually necessary to ensure the logical transition from the physical DC power system to the system matrix, whose study leads to the poles positioning in the Gauss plane. As well known, the poles position (i.e. right/left part of real axis) is representative of the stability performance (i.e. unstable/stable behavior). The determination of these positions deserves therefore a notable importance when investigating how a controlled DC power system plays in terms of stability.

The methodology of Section 19.3.1 is depicted in Figure 19.4 where different models are consequently obtained to reach the final numerical determination of poles positioning, thus the stability performance as an outcome. The flowchart proposed in the following is necessary to explain the methodology. In such a flowchart, a particular attention is put on models by providing remarks on their definition and validation.

19.3.1 Stability assessment flowchart

In the past, important contributions like [59] have demonstrated how impedance and Eigenvalue Based Method (EBM) are equivalent in studying the DC stability, thus returning comparable results. By starting from this consideration, the proposed methodology is devoted in applying the eigenvalues' study [60–63], albeit opening to the possibility of others equivalent methodologies if adopting the impedance method.

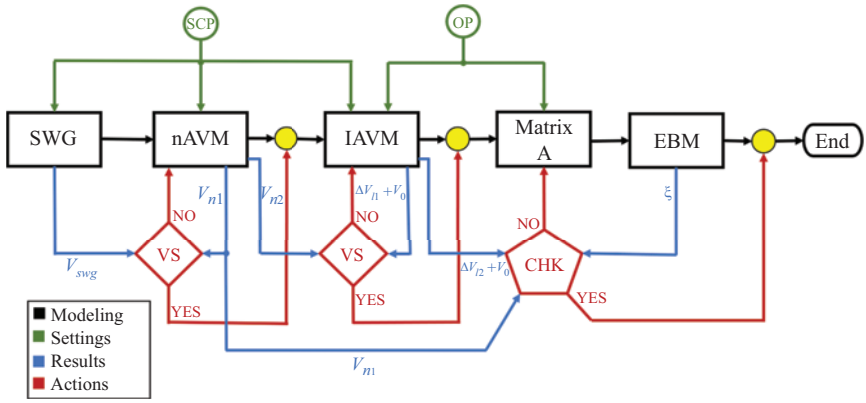

Figure 19.4 Stability assessment flowchart [53]

As known, the eigenvalue method is based on the definition of the analytical state-space matrix of the system. Consequently, the first assumption is related to the modeling data: the complete knowledge about the system is the starting point prior the mathematical modeling. In this work, all the system parameters are sufficiently known by hypothesis, therefore the state space matrix can be definable with a convenient margin of error. Basing on this, the flow chart in Figure 19.4 wants to provide the step-by-step path from the system definition towards the final poles determination. The procedure [53] to investigate the stability behavior relies on transients comparisons, where only a sufficient correspondence can enable the next stage of modeling. In the proposed flowchart, three colors are adopted to express the multi-model methodology. The subsequent models or methods are highlighted in black squares, where for example SWG stands for switching model or EBM represents the Eigenvalue Based Method to find the poles. The green color is used to express the system settings and data, then subdivided in system and control parameters (SCP*) and operating points (OP). The blue color shows the numerical simulations, which provides the data for performing the comparison (VS*) in red blocks. In red also, the final check (CHK*) prior the flowchart end. To cover the flowchart, it is possible to observe the following steps. From the SCP (i.e. filters parameters, power converters characterization, control constants, distribution topology), the switching model (SWG) is built as a circuital power scheme. In this regard, the proposed study utilizes the potentiality offered by PSCAD™ environment. Evidently other dynamics simulations tools can provide equivalent results. The two models named nonlinear average value model (nAVM) and linearized average value model (lAVM) are direct consequence of SWG modeling. Although focusing on the only average values (i.e. the power converters' switching is neglected), the nAVM is aimed at clearly representing the nonlinear interactions which are at the basis of SWG functioning. Then, the linearized lAVM is

*SCP, VS and CHK are acronyms of 'system and control parameters', 'comparison' and 'final check', respectively.

the direct consequence, when the equations of nAVM are linearized in the nearby of the equilibrium point (OP). Each modeling step is feedback verified by contrasting the blue output. When the red blocks (VS) confirm the conformity, it is possible to overcome the yellow circles checkpoints. Finally, the state-space matrix and the EBM eigenvalues are the final outputs to conclude about the system stability. Models, checkpoints, and outputs are explained in the following.

19.3.2 Models for stability study

As a matter of fact, different are the possibility for modeling a controlled DC grid. Each path in modeling is strictly dependent on the final target. The proposed path is the one for reaching the identification of system poles. Other goals are conversely obtained by following other alternatives in modeling. This section explains all the consequent steps to ensure the transition from the circuital model to the linearized system on which identify the matrix. The initial topology of a DC power system (in the next sections some examples will be discussed in detail) is the case which develops the circuital model. In authors experience, the latter can be obtained in PSCAD environment, being this simulation software able to accurately model the power converters by taking also into account switching phenomena. This SWG model is the closest to the effective power system behavior, therefore it constitutes the reference for the subsequent verifications/validations on the resulting nAVM model (Figure 19.4). As the dynamics under study is usually distant (i.e. at least one decade for the separation in bandwidths) from the AC control on generation side, ideal voltage generators are usually considered as sources of the interfaces to the DC bus. This assumption is quite common in the modeling of islanded DC microgrids, indeed other examples on this issue are in [25,27,58]. Differently, the SWG representation can model the action of storage systems, when their interface converters react with a dynamics comparable to the one achieved on DC distribution power electronics. Once modeled the power grid and the control on power converters, the SWG model can provide the first transient of interest. When the DC power grid under study presents a radial topology, the main bus voltage transient V_{swg} after a perturbation is the output to be considered from the SWG model. Conversely, in zonal topology, two approaches are possible. The first one declares one bus as dominant, so the related voltage transient constitutes the output from the SWG model. Instead, a second approach identifies several bus voltages as important in the zonal distribution. In this case, the comparisons to validate the models are to be replied on different V_{swg_k} inputs, then evidently complicating the analysis.

As in Figure 19.4, the SCPs are the initial inputs for the creation of the nAVM model. These parameters describe the only beginning point that builds the mathematical development. Second important issue in the nAVM representation is the one related to the AVM hypothesis. As suggested in [13], also this methodology wants to disregard the switching behavior of power converters. By putting this assumption, the converters' dynamics operations can be synthesized in mathematical equations thus opening the curtain toward the analytical modeling. Being the presence of nonlinear switching hardly to be modeled in mathematical equations, therefore this assumption

plays a crucial role when pursuing a convenient mathematical representation of the investigated phenomena. From the knowledge about system distribution (i.e. power system's components, components' topology, power converters, control laws), a set of nonlinear differential equations can be written to represent the dynamics operation of the DC microgrid. This set of equations is conveniently defined by considering two aspects. A certain number of equations is directly obtainable by solving the power scheme thanks to the Kirchhoff's circuit laws. Conversely, a second group depends on the control laws, therefore the regulating signals implemented by the power electronics actuators. By combining these two groups, a final set of nonlinear equations describes the nAVM model. In authors experience, the Simulink® is a convenient tool for modeling the nAVM, especially when the integrators are made explicit to easily managing the differential equations. By forcing the same load step in the numerical model on Simulink as well as in the SWG on PSCAD, the nAVM dynamic response on the bus voltage V_{n1} is put in comparison (Figure 19.4) with the V_{swg} from the SWG model. When the nAVM transient corresponds to the average value of the switching one, then the nAVM model is validated so it can behaves as new reference for the next verification with linearized lAVM model. If this check is not verified, then the nAVM must be corrected up to provide a transient that corresponds to the mean value of the PSCAD evolution.

Finally, the lAVM model is the third outcome. As in Figure 19.4, such a linearized model is developed by considering the nonlinear equations of nAVM and the operating points (OP). To linearize the nAVM equations, the classical method foresees a sequence of partial derivatives in a set of stable operating points. The latter are constituted by the state variables (e.g. voltages, currents, duty cycles) in steady-state conditions. In the nAVM Simulink model, they represent the steady-state values that are visible at the integrators' outputs once the transient is concluded. In this regard, a consideration is consequent when taking into account the system perturbation (e.g. load step). To propose an accurate model, the equilibrium points are to be calculated in two scenarios, both before and after the perturbation. To perform the linearization, the nonlinear equations of nAVM are initially gathered as $\frac{d}{dt}x = f(x,u)$. In last equation, x are the state variables while u is utilized to represent the system inputs (e.g. voltage references, ideal voltages to supply the DC interfaces). When the nonlinear equations are linearized in the stable equilibrium points, the resulting model equations become effective in small-signal conditions (i.e. small perturbations around the steady-state condition) and they take the new linearized representation as in $\frac{d}{dt}\Delta x = \tilde{A} \cdot \Delta x + B \cdot \Delta u$. In last equation, $\tilde{A}$ and B are the matrices to precisely describe the linearized system. Being constant the inputs on the system, the B matrix is null. After the linearized lAVM model is defined, an important test is now requested to verify its correctness then proceeding in the multi-model stability assessment. In particular, an evaluation wants to compare two transients from nAVM and lAVM. As the validity of nAVM model has been already proven by the SWG correspondence, the nAVM can play as benchmark for the comparison with lAVM in terms of dynamics transients. To check the lAVM model against the nAVM one, the same small-perturbation (-10% on bus voltage) acts on both models implemented on Simulink tool. Particularly, by changing the initial condition on system's aggregated

integrator (i.e. cumulative capacitance in radial distribution), the starting voltage value on the main bus voltage is accordingly modifiable in both models. As in Figure 19.4, the nAVM and the lAVM voltage transients (i.e. V_{n2} and $\Delta V_{l1} + V_0$) are now compared in the CHK checkpoint. When the transients are sufficiently similar, the two models behave as equivalent in the nearby of operating points. In this condition, the linearized state matrix is attainable from the lAVM for the stability study. Differently, the lAVM model needs a review and possibly some modifications.

19.3.3 State-space matrix

The final step of the multi-model methodology is related to the output of linearization process, thus the state-space $\tilde{A}$ matrix . The importance of this matrix is notable, as the study on $\tilde{A}$ can identify the poles position, so finally the stability performance of the DC system under investigation. As expressed before, the $\tilde{A}$ matrix is to be defined in two different conditions. Indeed, as the operating points are modified by the perturbation, consequently also the matrix's parameters change. In other words, one matrix is to be intended for the operation before the perturbation (i.e. load step), a second one for the analysis after the load increase. Once the matrices are ready to be studied, the EBM block numerically extracts the eigenvalues, thus finally defining the system poles. The analysis of the eigenvalues of these two matrices is effective to investigate the small-signal stability of the system before and after the perturbation. As well known from control theory, all the real part of eigenvalues must be negative for ensuring stable evolutions in the nearby of a precise operating point (i.e. the one in which the $\tilde{A}$ is calculated). In other words, a single eigenvalue with a positive real part is sufficient for an unstable behavior. The importance of these eigenvalues is therefore prominent, as well as the logical steps to find them. Additionally, the EBM at the final step is also able to identify the ξ damping factor, by observing the real part of the most critical poles, thus the ones more oriented on the right (unstable) plane.

Besides these important conclusions about stability, an additional confirmation is necessary to have the certainty about $\tilde{A}$ definition. A cross check between the information from EBM and the dynamics evolutions of both the nAVM and lAVM is therefore performed as visible in Figure 19.4. Also in this case, a step down on initial bus voltage condition (i.e. −10%) is adopted to close the discussion on nAVM, lAVM and $\tilde{A}$. Therefore, the stability assessment on $\tilde{A}$ eigenvalues is compared to the dynamic information coming from the nAVM and lAVM models, thus V_{n1} and $\Delta V_{l2} + V_0$ transients. Again, if the matrix eigenvalues have always negative real part, then both nAVM and lAVM models must experience a stable evolution toward the new operating point. When only one eigenvalue is characterized by a positive real part, thus the unstable evolutions must be made evident in nAVM and lAVM transients. In such a comparison, the ξ damping factor is also convenient for quickly glimpsing unstable conditions (i.e. negative damping factor). As said before, if this final verification is not positive, then certainly the construction of $\tilde{A}$ matrix or EBM algorithm are failed as the other models (i.e. nAVM and lAVM) are already verified thanks to the step-by-step methodology. The identification of system eigenvalues is at the end capable of giving the final check on system stability. On the other

hand, the numerical assessment on the dynamics transients provides the proof about the modeling accuracy. Evidently, the choice of building partial-consecutive models is successful being fostered the error identification if necessary. The multi-model methodology flowchart is applicable to several DC controlled distributions. When modifying the system topology (e.g. moving from radial to zonal distribution), the only modification regards the mathematical model which ever must be sufficiently accurate to correctly approximate the real system behavior.

19.4 Application on DC microgrids

The present section is aimed at applying the multi-model methodology [53] on the DC distribution in Figure 19.5. The proposed power scheme is related to a controlled MVDC microgrid to be implemented on ships. Again, the marine context imposes a particular attention on the stability issues giving the intrinsic isolated operation. In DC systems, the large presence of controlled interface converters and relative filters actually constitute the perfect environment in which a small perturbation can trigger the destabilizing oscillations. Such an effect depends on the filtering arrangements and on the control performance to be ensured by the converters. This section considers both aspects when locating the poles by EBM.

19.4.1 Power system design

The advanced control of DC microgrids is achieved only in presence of a large employment of power electronics. For this reason, the radial distribution in Figure 19.5 shows

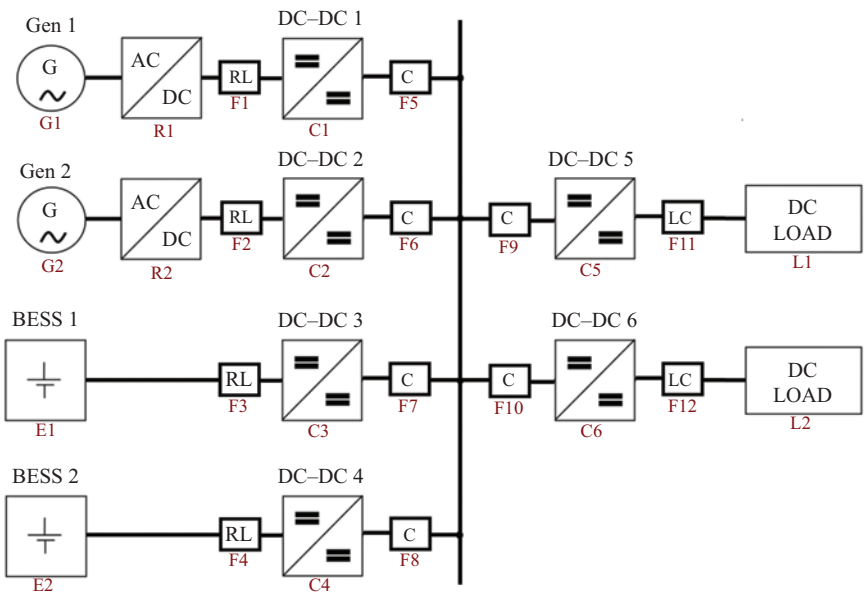

Figure 19.5 Radial multiconverter DC microgrid on ships [53]

several converters to interface the different elements to the common DC bus [53]. In the generating section on the left, two cascades of diode rectifiers (R1–R2) and DC–DC boost converters (C1–C2) are utilized to supply the grid from diesel generators (G1–G2). The storage function is given by E1–E2, the two battery energy storage systems (BESS). Their output voltage is adapted to the DC bus value thanks to two DC–DC buck-boost converters (C3–C4). On the load side, two DC–DC step-down buck converters (C5–C6) are in charge of feeding the two equivalent DC loads. These resistive terms are sufficiently accurate in aggregating the onboard loads. The data for the power converters design [53] are in Table 19.1, where the k subscript identifies the k-quantity or parameter for each component of the system. Then, the f_s is the switching frequency, V_{ACk} is the synchronous machine line–line output voltage, V_{DCk} represents the battery rated output and V_k the DC load rated voltage. To complete the information, P_{nk} is the converter rated power, V_n is the rated bus voltage, and I_{nk} the rated inductor current. Finally, R_{nk} models the rated load, while the converter control signal in nominal condition is named u_{nk}. To ensure the power quality requirements [13], each converter is equipped with its own input (F1–F4, F9–F10) and output (F5–F8, F11–F12) filter. An ohmic-inductive filter (R_{fk} and L_{fk}) is put at the input of diode rectifiers and batteries. For the C1–C2 converters, this filter resistor takes into account the converter losses. Differently, it models the battery internal resistance for C3–C4. In the DC system, each power converter has its own capacitor facing the bus. All the capacitors are thus parallel connected then summed in a single C_{BUS} capacitance. For the load converters (C5–C6), an LC filter is installed at the output, then C_{fk} and L_{fk} are the parameters once neglected the filter resistance. The onboard filters are in Table 19.2, while the design guidelines are in [64–67]. Attention is to be spent on the last two lines of the table. By assuming that a single converter is supplying its rated power to a CPL, the ω_{0fk} natural frequency and ξ_{fk} damping factor are two indices (Table 19.2) to weigh how the single filter impact on stability. Although the CPL is a pejorative assumption and this simplified evaluation considers each single converter as independent, a very negative damping factor (e.g. less than -0.5) anyway means the need of actions. An increment in capacitive filter or the control by linearizing functions can be crucial solutions.

Table 19.1 Design of DC–DC power converters [53]

	C1/C2	**C3/C4**	**C5**	**C6**
f_s [Hz]	3000	3000	3000	3000
V_{Ack} [V]	850	–	–	–
V_{Dck} [V]	–	1200	–	–
V_k [V]	–	–	1300	1300
P_{nk} [MW]	3	1	3	5
V_n [V]	1500	1500	1500	1500
I_{nk} [A]	2500	833	2308	3846
R_{nk} [Ω]	0.75	2.25	0.563	0.338
u_{nk}	0.2	0.2	0.867	0.867

Table 19.2 Design of filtering arrangements [53]

	C1/C2	**C3/C4**	**C5**	**C6**
Type	Boost	Buck-boost	Buck	
R_{fk} [mΩ]	35	85	–	–
L_{fk} [mH]	0.2	0.2	0.103	0.062
C_{fk} [mF]	–	–	0.360	0.560
C_{DCk} [mF]	6.0	6.0	6.0	6.0
ω_{0fk} [rad/s]	730	730	5193	5366
ξ_{fk}	–0.032	0.24	–0.37	–0.49

Table 19.3 Design of control bandwidths [53]

	I	**II**
Current controller C1–C2 [rad/s]	100	125
Bus voltage controller C3–C4 [rad/s]	10	220
Load voltage controller C5–C6 [rad/s]	1000	1000

19.4.2 Control design

In DC microgrids, the coordination of control tasks is essential and each converter must provide a specific work. In Figure 19.5, C3–C4 are indeed responsible for the bus voltage regulation in droop mode while ensuring an equal power sharing (i.e. $R_{dp} = 0.01\Omega$). This value is sufficient to have both dynamic decoupling and limited voltage drop in full power condition. Then, C1–C2 are current controlled and C5–C6 regulate the voltages on their own loads. To make the system equations more manageable, the control loop of each converter is based on the only action of an integral regulator. Although this assumption can appear simplistic, this control can properly command the converters action in voltages/currents regulation. The integral gain of each loop is individually tuned to ensure the requested control bandwidth. Then, the dynamics coherence is verified by identifying the time constants on reference step tests. Table 19.3 shows two combinations of control bandwidths. The first (I) is imposed to ensure the stability after the perturbation. In this case, the three control loops are dynamically decoupled. The second combination (II) is conversely conceived to experiment an unstable condition. In this case, not only the decoupling is lost but also the system poles are voluntarily put on the *y*-axis in the Gauss plane. This constitutes a sort of test for understanding the performance limit before dealing with instability. By performing the tests on these combinations, it is possible to verify the effective correspondence between poles location and simulated transients:

$$\begin{aligned}\frac{d}{dt}V_{DC}(t) = \frac{1}{C_{BUS}} \cdot \big[&\big(1 - D_1(t)\big) \cdot I_1(t) + \big(1 - D_2(t)\big) \cdot I_2(t) + \\ &+ \big(1 - D_3(t)\big) \cdot I_3(t) + \big(1 - D_4(t)\big) \cdot I_4(t) + \\ &- D_5(t) \cdot I_5(t) - D_6(t) \cdot I_6(t)\end{aligned} \tag{19.1}$$

$$\frac{d}{dt}I_1(t) = \frac{1}{L_1} \cdot \left[V_{RT1} - \left(1 - D_1(t)\right) \cdot V_{DC}(t) - R_1 \cdot I_1(t)\right] \tag{19.2}$$

$$\frac{d}{dt}D_1(t) = K_{i1} \cdot \left[{I_1}^* - \left(1 - D_1(t)\right) \cdot I_1(t)\right] \tag{19.3}$$

$$\frac{d}{dt}I_2(t) = \frac{1}{L_2} \cdot \left[V_{RT2} - \left(1 - D_2(t)\right) \cdot V_{DC}(t) - R_2 \cdot I_2(t)\right] \tag{19.4}$$

$$\frac{d}{dt}D_2(t) = K_{i2} \cdot \left[{I_2}^* - \left(1 - D_2(t)\right) \cdot I_2(t)\right] \tag{19.5}$$

$$\frac{d}{dt}I_3(t) = \frac{1}{L_3} \cdot \left[V_{BT3} - \left(1 - D_3(t)\right) \cdot V_{DC}(t) - R_3 \cdot I_3(t)\right] \tag{19.6}$$

$$\frac{d}{dt}D_3(t) = K_{i3} \cdot \left[{V_{DC}}^* - V_{DC}(t) - R_{dp} \cdot \left(1 - D_3(t)\right) \cdot I_3(t)\right] \tag{19.7}$$

$$\frac{d}{dt}I_4(t) = \frac{1}{L_4} \cdot \left[V_{BT4} - \left(1 - D_4(t)\right) \cdot V_{DC}(t) - R_4 \cdot I_4(t)\right] \tag{19.8}$$

$$\frac{d}{dt}D_4(t) = K_{i4} \cdot \left[{V_{DC}}^* - V_{DC}(t) - R_{dp} \cdot \left(1 - D_4(t)\right) \cdot I_4(t)\right] \tag{19.9}$$

$$\frac{d}{dt}V_5(t) = \frac{1}{C_5} \cdot \left[I_5(t) - \frac{V_5(t)}{R_{L1}}\right] \tag{19.10}$$

$$\frac{d}{dt}I_5(t) = \frac{1}{L_5} \cdot \left[D_5(t) \cdot V_{DC}(t) - V_5(t)\right] \tag{19.11}$$

$$\frac{d}{dt}D_5(t) = K_{i5} \cdot \left[{V_5}^* - V_5(t)\right] \tag{19.12}$$

$$\frac{d}{dt}V_6(t) = \frac{1}{C_6} \cdot \left[I_6(t) - \frac{V_6(t)}{R_{L2}}\right] \tag{19.13}$$

$$\frac{d}{dt}I_6(t) = \frac{1}{L_6} \cdot \left[D_6(t) \cdot V_{DC}(t) - V_6(t)\right] \tag{19.14}$$

$$\frac{d}{dt}D_6(t) = K_{i6} \cdot \left[{V_6}^* - V_6(t)\right] \tag{19.15}$$

19.4.3 Average value models

Once neglected the converters switching, (19.1)–(19.15) models the grid in Figure 19.5. This model preserves the nonlinear behavior, but it considers the only mean value of electrical quantities. The equations of each converter (C1–C6) are at the basis of the model. The common DC bus voltage is named V_{DC}, while the single current in the converter inductance is I_k. Each DC–DC converter is regulated by a duty cycle named D_k. In all the control loops acting on converters, the only integral coefficient K_{ik} is adopted, whereas the terms with asterisk are the references. To simplify the modeling, the V_{RTk} output of rectifiers is constant like the V_{BTk} output of batteries. The voltage on R_{Lk} load is named V_k. By combining (19.1)–(19.15), the nAVM numerical model is built in Simulink. From nAVM and equilibrium points $[V_{DC0}, I_{k0}, D_{k0}, V_{k0}]$,

the linearization by partial derivatives defines the lAVM as in [54]. Also, this model is then implemented in Simulink.

19.4.4 Poles location

The small-signal stability of the controlled DC grid (Figure 19.5) is assessed by locating the system poles in the $\mathbb{C}$ plane [53,54]. Such an evaluation wants to verify how the control bandwidths impact on poles positioning. In this test, the DC grid parameters are in Tables 19.1 and 19.2. From the initial condition where the C5–C6 high-bandwidth (i.e. 1000 rad/s) converters provide 2 MW and 1.5 MW, respectively, an additional step request of 2 MW from C6 is the way to perturb the system. The performed analysis demonstrates how this perturbation cannot move the poles in the right plane when the system is controlled with tight and decoupled bandwidths (I). Conversely, the same perturbation triggers the instability if high performance (i.e. 220 vs. 10 rad/s) is requested on the bus voltage dynamics as in (II) combination. Thanks to the multi-model methodology and its consequent verifications on transients (Section 19.3.1), four lAVM models are defined to analyze the four cases. Thus, two lAVM models where the bandwidths are configured on combination (I), before and after the perturbation. Other two linearized models by setting on the (II) combination, in the first equilibrium point and in the second after the load step. From the lAVM models, the four matrices are analytically defined whereas the related eigenvalues are revealed by means of a numerical calculus. In the resulting representation in the Gauss plane, the complex conjugate poles are relevant for the stability matter, as they can experiment the shifting in the right half plane after the load increase. Conversely, the real poles are always on the stable plane, whichever the control bandwidths are. Figure 19.6 shows the poles with the (I) combination of bandwidths (100-10-1000 rad/s). Both before and after the step, all the poles have negative real parts, thus disclosing system stability. Instead, the poles with the (II) bandwidths combination (125-220-1000 rad/s) are in Figure 19.7. The rise in voltage-current control bandwidths force a pair of complex poles in passing the y-axis. Particularly, the focus is on the complex poles related to the bus capacitance. Before the load step, the stability is confirmed by their negative (-7) real part. Differently, the instability arises when their real part becomes positive (6) after the perturbation.

19.4.5 Numerical verification

The poles location is the method to envisage the possible reasons for microgrid instability (e.g. high-performance control, not-integrated filters design). Once identified the cause, the DC grid can be redesigned (e.g. reduction in control performance, increase in capacitive terms) to host the poles in the left half plane, thus ensuring the stability. As the location of poles is the result of a complex analytical-numerical process, the errors in modeling are quite common. A validation is thus unavoidable to verify the coherence between poles position and simulated transients. This section proposes the transients in Figures 19.8–19.13 to check the poles location. To provide an effective verification, each figure has the switching transients from SWG models in PSCAD and also the ones by running the nAVM models in Simulink. The results are in per-unit notation. The rated bus voltage (i.e. 1500 V) and the total generating

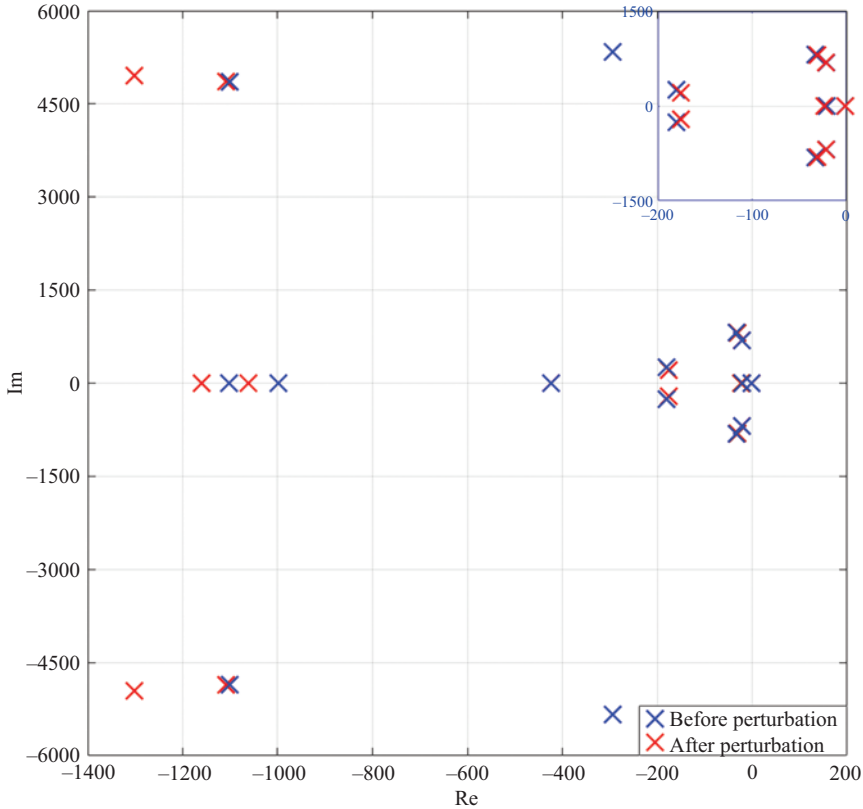

Figure 19.6 Poles location in the stable case, (I) bandwidths combination [53]

power (i.e. 8 MW) are the main bases, while the current is rescaled as a consequence (Table 19.1). For more clarity, only the per-unit of load voltage is referred to its own rated value (1300 V). To validate the EBM analysis on poles, Figures 19.8 and 19.9 give the DC bus voltage responses to the load increase at 0.7 s. The (I) combination is adopted in the transients of Figure 19.8, while the destabilizing combination (II) configures the systems simulated in Figure 19.9. As foreseen by poles location, when the control loops are set on (I) bandwidths, the stability is guaranteed even after the perturbation (Figure 19.8). Here, the voltage drop after the load increase is near −9%, then validating the small-signal assumption. Then, at steady-state the voltage settles at 0.995 p.u. due to the droop control. On the other hand, the unstable behavior predicted by the poles location is made evident also in the dynamics transients. Indeed, Figure 19.9 displays how the instability is triggered by the same perturbation that is responsible for the complex poles' repositioning in the right half plane (Figure 19.7). The good correspondence between switching (SWG) and average results (AVM) in Figures 19.8 and 19.9 is an additional verification on the validity of the multi-model methodology. To complete the study, also the power/current transients are provided

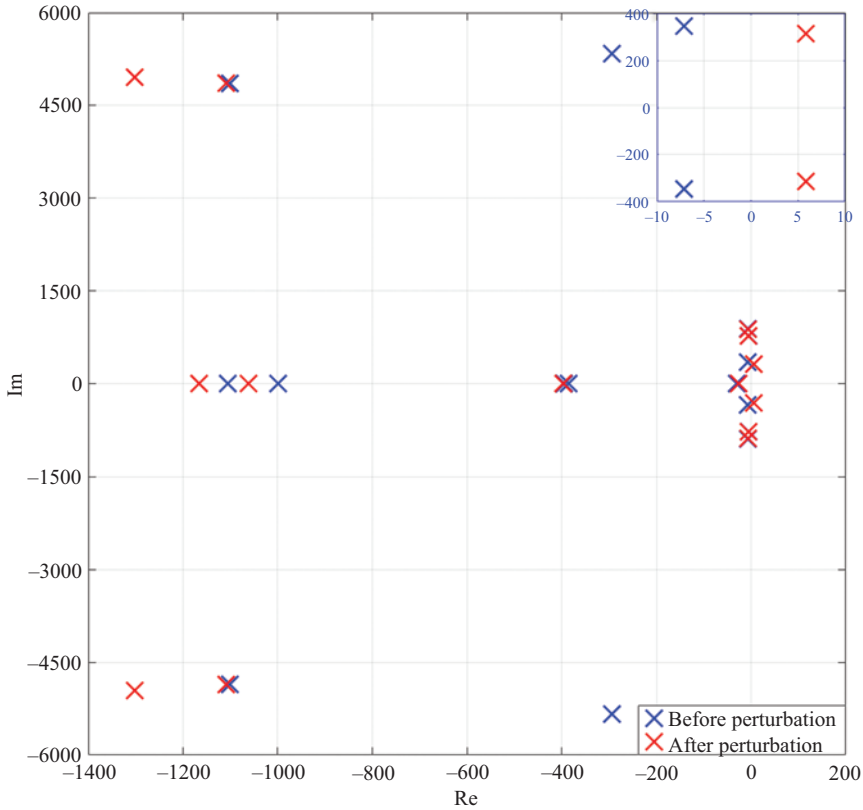

Figure 19.7 Poles location in the unstable case, (II) bandwidths combination [53]

for the stable case on (I) bandwidths configuration. Figure 19.10 shows the generating converters power, before and after the perturbation. At the initial steady-state, the C1–C2 current-controlled converters supply 3.5 MW (i.e. almost 0.45 p.u.) to the loads. This power is shared on the generating converters basing on their current references. Talking about the C3–C4 on BESS, at the beginning they do not furnish power being only responsible of controlling the bus voltage. Their overlapped transient shows no-power till the perturbation. At 0.7 s, the power from C6 (Figure 19.11) increases from 1.5 MW to 3.5 MW. As the bandwidth on current control is higher than the one on voltage control, then C1 and C2 are the first to react to this demand. Then the power shortage is supplied by C3–C4 as in Figure 19.10. As they control the bus voltage in droop mode, a slight reduction on this voltage is expectable (Figure 19.8) as well as a consequent small decrease in the powers from C1–C2 current-controlled converters. Therefore, C3–C4 must finally feed a little more than 1 MW each (i.e. 0.13 p.u.). Lastly, the C6 input current and output voltage are in Figures 19.12 and 19.13. In the last figure, the high-performance of C6 is evident where indeed the voltage is restored in about 2.5 ms after the load step.

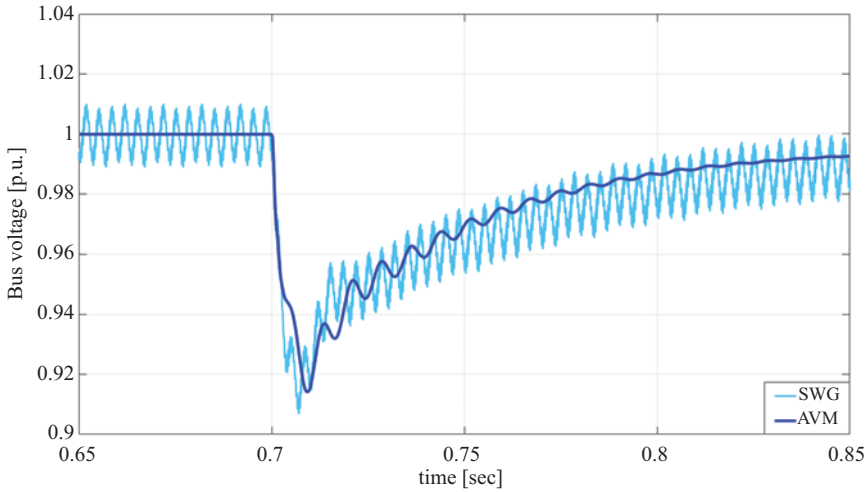

Figure 19.8 Bus voltage transient after perturbation, stable case [53]

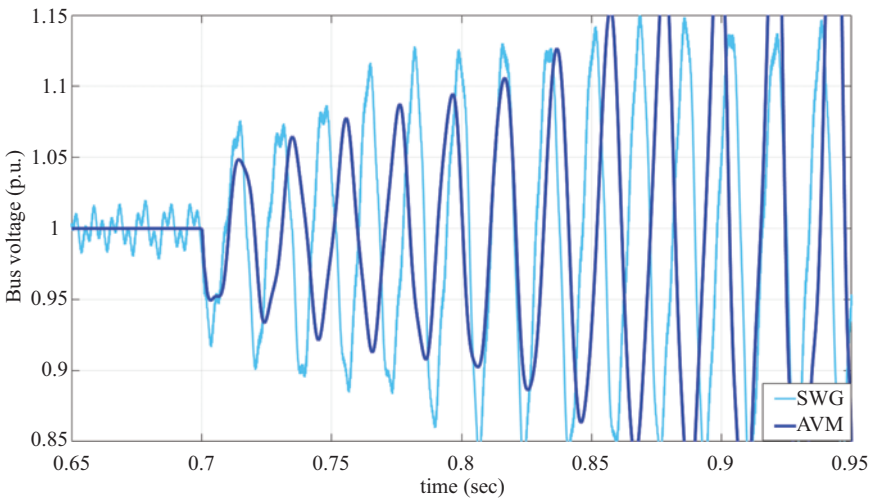

Figure 19.9 Bus voltage transient after perturbation, unstable case [53]

19.4.6 Considerations on stability assessment in zonal distribution

Since the early 2000, the DC technology has been the enabler for the zonal power systems on ships [45]. Nowadays, this distribution is the smartest way to manage the marine grids if seeking higher efficiency and redundancy [17,46]. As in Section 19.2.2, other advantages force towards the ZEDS implementation, for example

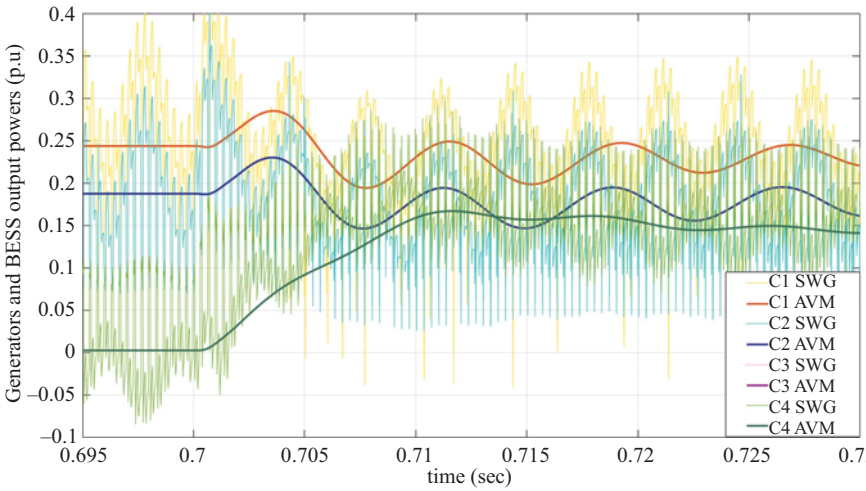

Figure 19.10 Output powers of generating converters [53]

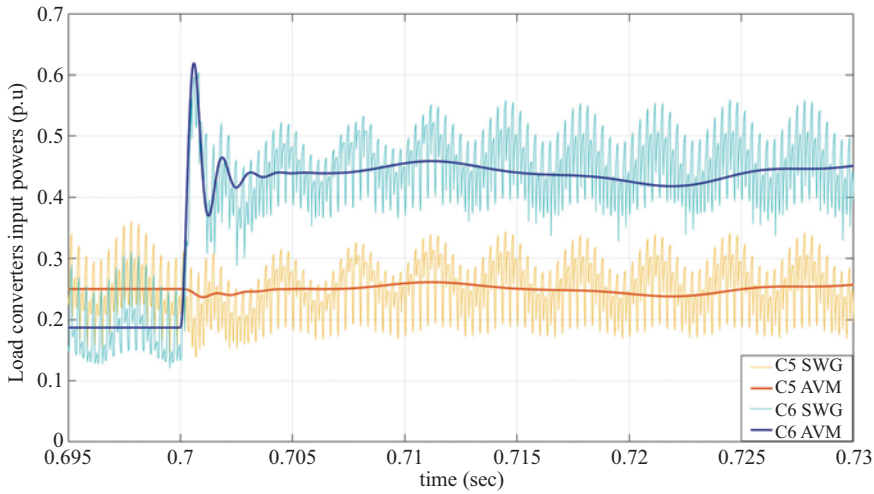

Figure 19.11 Input powers of load converters [53]

high reliability and advanced power management. Regarding the first, the controlled topology of ZEDS can avoid the disturbances propagation between distinct electrical zones. Considering the decoupling action of interface converters, the disturbances are not propagated between zones, neither when adjacent. The absence of propagation thus leads to reliability and feasibility. Second, the wide employment of power

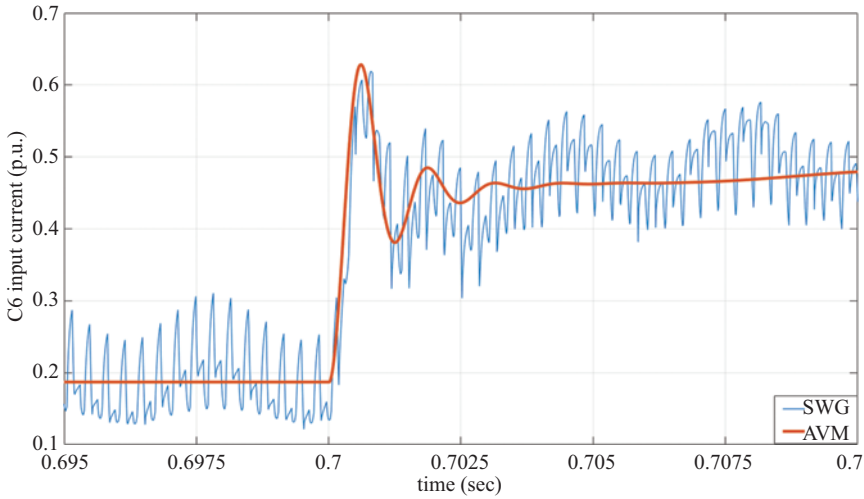

Figure 19.12 Input current of C6 converter [53]

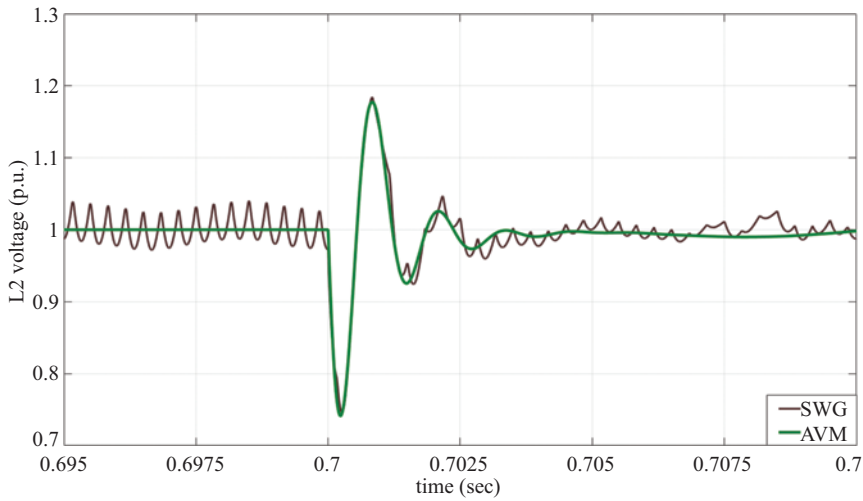

Figure 19.13 Voltage on L2 load [53]

converters improve the power flows between zones. Not only the convenient power sharing from the generating converters (the ones that interface the sources) is guaranteed, also the transient power from storage systems is optimized in order to ensure loads feeding and system stability, even in adverse conditions. A ZEDS is a power-enabler to maximize the operational capability, both in standard-operative and in extreme-faulty scenarios. As in [17,46], the ZEDS acts as a controlled distribution to feed the different sections of a system. Evidently, the main components of a ZEDS (i.e.

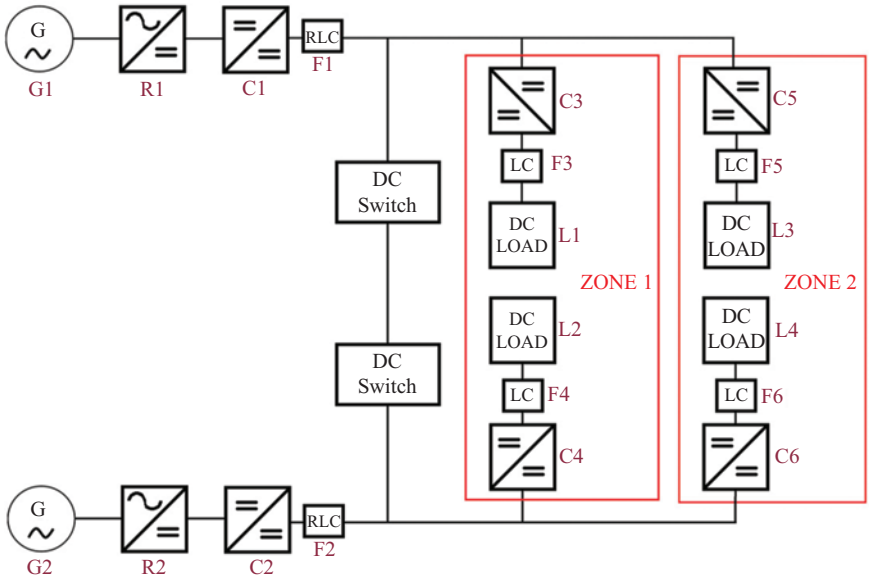

Figure 19.14 Zonal multiconverter DC microgrid on ships, disjointed configuration

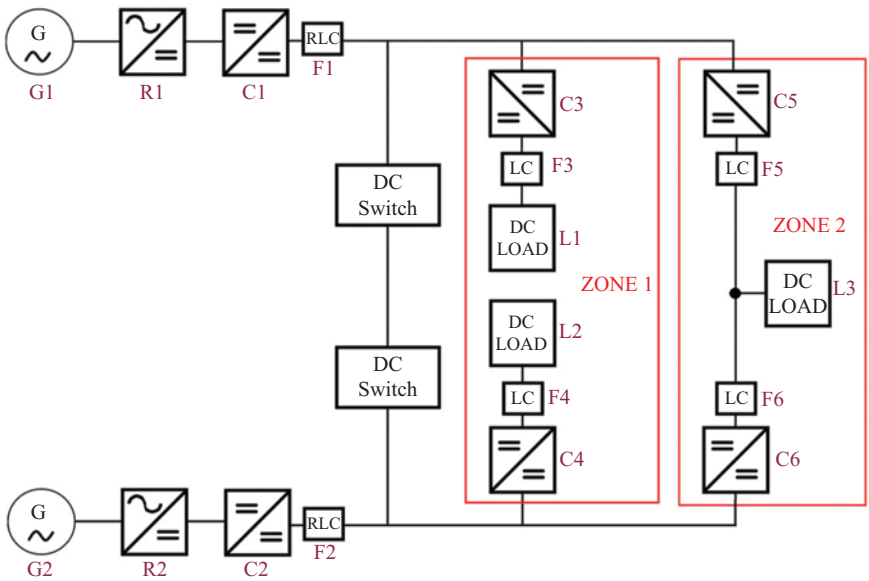

Figure 19.15 Zonal multiconverter DC microgrid on ships, parallel configuration

power converters, control systems, generation-storage systems and cables) ensures its power delivering to the loads. In general, a ZEDS does not contain its supplied loads. Conversely, the ZEDS and its loads constitute the so-called Zone, which is interfaced to the external by converters. Albeit the ZEDS does not include the loads, anyway it must ensure power quality and quality of service on the systems it supplies. As a ZEDS does not contain its loads [17,46], also the DC zonal systems on which evaluate the stability can have different configurations. By assuming the coherence with the guidelines in Section 19.2.2, two systems are identified to discuss about ZEDS implementation and stability study. The first case in Figure 19.14 is a disjointed configuration acting as zonal. The two loads in Zone 1 (L1–L2) are supplied from different converters (C3–C4), identical considerations for the loads in Zone 2. The four converters manage the power balance in the two zones, but the stability issue is after all correspondent to the one of a radial system. If the switches are opened, then L2–L4 are the paralleled loads of C2 and L1–L3 are the ones of C1. If the switches are closed the system remains radial, but all the load converters (C3–C4–C5–C6) are simultaneously fed by the two generating converters (C1–C2) in parallel. When approaching the stability analysis on the disjointed configuration, the same considerations of Sections 19.4.1–19.4.4 can be tailored on the zonal (radial) grids in Figure 19.14. Different remarks if the parallel configuration is adopted for the intrinsic DC zonal distribution (Figure 19.15). When the DC switch is open, L1–L2 are the radial loads for C1–C2, while L3 is paralleled fed by C5–C6. On the other hand, when the switch is closed, the unique bus supplies the radial loads L1–L2 and also the C5–C6. In turn, these converters supplies the L3 in parallel thus constituting a second distribution, whose voltage is controlled by C5–C6. The stability study on the distribution in Figure 19.15 thus needs a particular attention. Particularly, equations similar to (19.7) and (19.9) are to be written and integrated into the model in order to take into account both the two droop controlled distribution.

19.5 Conclusions

This chapter proposes a multi-model methodology to assess the system stability in advanced DC microgrids. As destabilizing behaviors are possible and dangerous in these LC filtered grids, a complete analysis based on poles location becomes pivotal, especially when the DC microgrids are islanded as in the marine context. Indeed, in these systems even small destabilizing perturbations on the bus can provoke the ship blackout caused by the intervention of over-under voltage protections. The problem is also significant in the DC microgrids on land, where the protections action means outages therefore loss of business. For these reasons, important efforts are invested on studying the DC stability, thus identifying both methods to investigate the nonlinear phenomenon and control techniques to compensate for the instability. This chapter is mainly oriented on the first target, thus it wants to provide a methodology to study the controlled grid and its criticality on the stability matter. To do this, the chapter describes a new way to assess the DC stability by means of an analytical–numerical

tool. The latter is capable to foresee the stability performance without the need of time-consuming emulations, thus a great advantage for whom is in charge of designing the microgrid. After a detailed description on radial and zonal DC distributions, the chapter introduces a flowchart to achieve the stability assessment of DC grids. The proposed methodology is mainly based on three consequent models. First, the switching model (SWG) is the circuital representation of the controlled system. As it faithfully reproduces the dynamics behavior of the actual DC grid, it is mainly used to verify the correspondence of next models. Once neglected the switching behavior on SWG, the nonlinear average value model (nAVM) is thus defined. Although this model is only capable of providing the mean value of electrical quantities, it results sufficiently accurate when investigating the system stability in presence of perturbations. The lAVM is then found by linearizing the nAVM in the stable equilibrium point in which the system operates in steady-state condition. Then, the state-space matrix is defined by taking into account the mathematical equations that are behind the lAVM model. By a numerical analysis on this matrix, the poles on which the system operates are localized in the Guass plane. When all the poles have negative real parts, the system stability is guaranteed. Conversely, even a single pole with positive real part means system instability. Dynamics tests on PSCAD and Simulink can finally validate the multi-model methodology by confirming its capability in predicting the instability. In conclusion, a radial converters-based DC grid is the study-case on which the proposed method verifies the influence of control bandwidths on stability. Additional considerations about DC zonal distribution are at the end necessary to enable the stability assessment on totally controlled flexible-resilient grids.

Acknowledgment

The authors wish to thank Prof. Giovanni Giadrossi and PhD student Andrea Alessia Tavagnutti for their valuable contribution in preparing this chapter.

Copyright notice

Bibliography

[1] N. Hatziargyriou, *Microgrids: Architectures and Control*, New York, NY: Wiley, 2014.

[2] T. Dragicevic, J. C. Vasquez, J. M. Guerrero, and D. Skrlec, Advanced LVDC electrical power architectures and microgrids: a step toward a new generation of power distribution networks, *IEEE Electrification Magazine*, vol. 2, no. 1, pp. 54–65, 2014.

[3] L. E. Zubieta, Are microgrids the future of energy? DC microgrids from concept to demonstration to deployment, *IEEE Electrification Magazine*, vol. 4, no. 2, pp. 37–44, 2016.

[4] M. Nasir, H. A. Khan, N. A. Zaffar, J. C. Vasquez, and J. M. Guerrero, Scalable solar dc micrigrids: on the path to revolutionizing the electrification architecture of developing communities, *IEEE Electrification Magazine*, vol. 6, no. 4, pp. 63–72, 2018.

[5] B. T. Patterson, DC, come home: DC microgrids and the birth of the internet, *IEEE Power and Energy Magazine*, vol. 10, no. 6, pp. 60–69, 2012.

[6] E. Rodriguez-Diaz, J. C. Vasquez, and J. M. Guerrero, Intelligent DC homes in future sustainable energy systems: when efficiency and intelligence work together, *IEEE Consumer Electronics Magazine*, vol. 5, no. 1, pp. 74–80, 2016.

[7] G. Sulligoi, A. Tessarolo, V. Benucci, A. Millerani Trapani, M. Baret and F. Luise, Shipboard power generation: design and development of a medium-voltage dc generation system, *IEEE Industry Applications Magazine*, vol. 19, no. 4, pp. 47–55, 2013.

[8] P. Cairoli and R. A. Dougal, New horizons in DC shipboard power systems: new fault protection strategies are essential to the adoption of DC power systems, *IEEE Electrification Magazine*, vol. 1 no. 2, pp. 38–45, 2013.

[9] M. R. Banaei and R. Alizadeh, Simulation-based modeling and power management of all-electric ships based on renewable energy generation using model predictive control strategy, *IEEE Intelligent Transportation Systems Magazine*, vol. 8, no. 2, pp. 90–103, 2016.

[10] Z. Jin, G. Sulligoi, R. Cuzner, L. Meng, J. C. Vasquez, and J. M. Guerrero, Next-generation shipboard DC power system: introduction smart grid and dc microgrid technologies into maritime electrical networks, *IEEE Electrification Magazine*, vol. 4, no. 2, pp. 45–57, 2016.

[11] D. Paul, A history of electric ship propulsion systems, *IEEE Industry Applications Magazine*, vol. 26, no. 6, pp. 9–19, 2020.

[12] G. Chang, Y. Wu, S. Shao, Z. Huang, and T. Long, DC bus systems for electrical ships: recent advances and analysis of a real case, *IEEE Electrification Magazine*, vol. 8, no. 3, pp. 28–39, 2020.

[13] IEEE Std 1709–2018 (Revision of IEEE Std 1709–2010), *IEEE Recommended Practice for 1 kV to 35 kV Medium-Voltage DC Power Systems on Ships*, pp. 1–54, 2018.

[14] D. Bosich, A. Vicenzutti, R. Pelaschiar, R. Menis, and G. Sulligoi, Toward the future: the MVDC large ship research program, *Proceedings of the 2015 AEIT International Annual Conference (AEIT)*, 2015, pp. 1–6.

[15] G. Sulligoi, A. Vicenzutti, and R. Menis, All-electric ship design: from electrical propulsion to integrated electrical and electronic power systems, *IEEE Transactions on Transportation Electrification*, vol. 2, no. 4, pp. 507–521, 2016.

[16] V. Bucci, U. la Monaca, D. Bosich, G. Sulligoi, and A. Pietra, Integrated ship design and CSI modeling: A new methodology for comparing onboard electrical distributions in the early-stage design, *Proceedings of the NAV2018 International Conference on Ship and Shipping Research*, Trieste, Italy, 20–22 June 2018; p. 124.

[17] IEEE Std 1826-2020 (Revision of IEEE Std 1826-2012), *IEEE Standard for Power Electronics Open System Interfaces in Zonal Electrical Distribution Systems Rated Above 100 kW*, pp. 1–44, 25 Nov. 2020.

[18] P. Kundur, *Power System Stability and Control*, McGraw-Hill, New York, NY, 1994.

[19] S. D. Sudhoff, K. A. Corzine, S. F. Glover, H. J. Hegner, and H. N. Robey, DC link stabilized field oriented control of electric propulsion systems, *IEEE Transactions on Energy Conversion*, vol. 13, no. 1, pp. 27–33, 1998.

[20] C. Rivetta, G. A. Williamson, and A. Emadi, Constant power loads and negative impedance instability in sea and undersea vehicles: statement of the problem and comprehensive large-signal solution, in *Proceedings of the IEEE Electric Ship Technologies Symposium*, 2005, pp. 313–320.

[21] C. H. Rivetta, A. Emadi, G. A. Williamson, R. Jayabalan, and B. Fahimi, Analysis and control of a buck DC–DC converter operating with constant power load in sea and undersea vehicles, *IEEE Transactions on Industry Applications*, vol. 42, no. 2, pp. 559–572, 2006.

[22] A. Kwasinski and C. N. Onwuchekwa, Dynamic behavior and stabilization of DC microgrids with instantaneous constant-power loads, *IEEE Transactions on Power Electronics*, vol. 26, no. 3, pp. 822–834, 2011.

[23] M. Cupelli, L. Zhu, and A. Monti, Why ideal constant power loads are not the worst case condition from a control standpoint, *IEEE Transactions on Smart Grid*, vol. 6, no. 6, pp. 2596–2606, 2015.

[24] A. M. Rahimi and A. Emadi, Active damping in DC/DC power electronic converters: a novel method to overcome the problems of constant power loads, *IEEE Transactions on Industrial Electronics*, vol. 56 no. 5, pp. 1428–1439, 2009.

[25] G. Sulligoi, D. Bosich, G. Giadrossi, L. Zhu, M. Cupelli, and A. Monti, Multiconverter medium voltage DC power systems on ships: constant-power loads instability solution using linearization via state feedback control, *IEEE Transactions on Smart Grid*, vol. 5, no. 5, pp. 2543–2552, 2014.

[26] X. Lu, K. Sun, J. M. Guerrero, J. C. Vasquez, L. Huang, and J. Wang, Stability enhancement based on virtual impedance for DC microgrids with constant

power loads, *IEEE Transactions on Smart Grid*, vol. 6, no. 6, pp. 2770–2783, 2015.

[27] D. Bosich, G. Sulligoi, E. Mocanu, and M. Gibescu, Medium voltage DC power systems on ships: an offline parameter estimation for tuning the controllers' linearizing function, *IEEE Transactions on Energy Conversion*, vol. 32, no. 2, pp. 748–758, 2017.

[28] X. Chang, Y. Li, X. Li, and X. Chen, An active damping method based on a supercapacitor energy storage system to overcome the destabilizing effect of instantaneous constant power loads in DC microgrids, *IEEE Transactions on Energy Conversion*, vol. 32, no. 1, pp. 36–47, 2017.

[29] M. A. Hassan and Y. He, Constant power load stabilization in DC microgrid systems using passivity-based control with nonlinear disturbance observer, *IEEE Access*, vol. 8, pp. 92393–92406, 2020.

[30] H. Wu, V. Pickert, M. Ma, B. Ji, and C. Zhang, Stability study and nonlinear analysis of DC–DC power converters with constant power loads at the fast timescale, *IEEE Journal of Emerging and Selected Topics in Power Electronics*, vol. 8, no. 4, pp. 3225–3236, 2020.

[31] M. S. Sadabadi and Q. Shafiee, Scalable robust voltage control of DC microgrids with uncertain constant power loads, *IEEE Transactions on Power Systems*, vol. 35, no. 1, pp. 508–515, 2020.

[32] M. Srinivasan and A. Kwasinski, Control analysis of parallel DC–DC converters in a DC microgrid with constant power loads, *International Journal of Electrical Power and Energy Systems*, vol. 122, p. 106207, 2020.

[33] Y. Gui, R. Han, J. M. Guerrero, J. C. Vasquez, B. Wei, and W. Kim, Large-signal stability improvement of DC–DC converters in DC microgrid, *IEEE Transactions on Energy Conversion*, vol. 36, no. 3, pp. 2534–2544, 2021.

[34] S. Pastore, D. Bosich, and G. Sulligoi, Influence of DC–DC load converter control bandwidth on small-signal voltage stability in MVDC power systems, in *Proceedings of the 2016 International Conference on Electrical Systems for Aircraft, Railway, Ship Propulsion and Road Vehicles & International Transportation Electrification Conference (ESARS-ITEC)*, 2016, pp. 1–6.

[35] S. Pastore, D. Bosich, and G. Sulligoi, Analysis of small-signal voltage stability for a reduced-order cascade-connected MVDC power system, in *Proceedings of the IECON 2017 – 43rd Annual Conference of the IEEE Industrial Electronics Society*, 2017, pp. 6771–6776.

[36] S. Pastore, D. Bosich, and G. Sulligoi, A frequency analysis of the small-signal voltage model of a MVDC power system with two cascade DC-DC converters, in *Proceedings of the 2018 IEEE International Conference on Electrical Systems for Aircraft, Railway, Ship Propulsion and Road Vehicles & International Transportation Electrification Conference (ESARS-ITEC)*, 2018, pp. 1–6.

[37] S. Pastore, D. Bosich, and G. Sulligoi, An analysis of the small-signal voltage stability in MVDC power systems with two cascade controlled DC–DC converters, in *Proceedings of the IECON 2018 – 44th Annual Conference of the IEEE Industrial Electronics Society*, 2018, pp. 3383–3388.

[38] D. Bosich and G. Sulligoi, Stability-oriented filter design optimization in cascade-connected MVDC shipboard power system, *Proceedings of the 2020 IEEE Power & Energy Society General Meeting (PESGM)*, 2020, pp. 1–5.

[39] U. Javaid, F. D. Freijedo, D. Dujic, and W. van der Merwe, MVDC supply technologies for marine electrical distribution systems, *CPSS Transactions on Power Electronics and Applications*, vol. 3, no. 1 pp. 65–76, 2018.

[40] IEC/IEEE International Standard – utility connections in port, Part 1: high voltage shore connection (HVSC) systems – general requirements, in *IEC/IEEE* 80005-1:2019 , pp. 1–78, 18 March 2019.

[41] IEC/IEEE International Standard – utility connections in port, Part 2: high and low voltage shore connection systems – data communication for monitoring and control, in *IEC/IEEE* 80005-2 Edition 1.0 2016-06, pp. 1–116, 27 June 2016.

[42] G. Sulligoi, D. Bosich, R. Pelaschiar, G. Lipardi, and F. Tosato, Shore-to-ship power, in *Proceedings of the IEEE*, vol. 103, no. 12, pp. 2381–2400, 2015.

[43] IEEE Std 1662-2016 (Revision of IEEE Std 1662-2008), *IEEE Recommended Practice for the Design and Application of Power Electronics in Electrical Power Systems*, pp. 1–68, 9 March 2017.

[44] IEEE Std 1676-2010, *IEEE Guide for Control Architecture for High Power Electronics (1 MW and Greater) Used in Electric Power Transmission and Distribution Systems*, pp. 1–47, 11 Feb. 2011.

[45] J. G. Ciezki and R. W. Ashton, Selection and stability issues associated with a navy shipboard DC zonal electric distribution system, *IEEE Transactions on Power Delivery*, vol. 15, no. 2, pp. 665–669, April 2000.

[46] G. Sulligoi, D. Bosich, A. Vicenzutti, and Y. Khersonsky, Design of zonal electrical distribution systems for ships and oil platforms: control systems and protections, *IEEE Transactions on Industry Applications*, vol. 56, no. 5, pp. 5656–5669, 2020.

[47] P. Kankanala, S. C. Srivastava, A. K. Srivastava, and N. N. Schulz, Optimal control of voltage and power in a multi-zonal MVDC shipboard power system, *IEEE Transactions on Power Systems*, vol. 27, no. 2, pp. 642–650, 2012.

[48] M. M. Biswas, T. Deese, J. Langston, *et al*., Shipboard zonal load center modeling and characterization on real-time simulation platform, in *Proceedings of the 2021 IEEE Electric Ship Technologies Symposium (ESTS)*, 2021.

[49] T. V. Vu, D. Gonsoulin, D. Perkins, B. Papari, H. Vahedi, and C. S. Edrington, in *Distributed Control Implementation for Zonal MVDC Ship Power Systems*, *Proceedings of the 2017 IEEE Electric Ship Technologies Symposium (ESTS)*, 2017.

[50] D. Perkins, T. Vu, H. Vahedi, and C. S. Edrington, Distributed power management implementation for zonal MVDC ship power systems, in *Proceedings of the IECON 2018 – 44th Annual Conference of the IEEE Industrial Electronics Society*, 2018.

[51] S. Chen, J. Daozhuo, L. Wentao, and W. Yufen, An overview of the application of DC zonal distribution system in shipboard integrated power system, in *Proceedings of the 2012 Third International Conference on Digital Manufacturing & Automation*, 2012, pp. 206–209.

[52] M. Ahmed, L. Meegahapola, A. Vahidnia, and M. Datta, Stability and control aspects of microgrid architectures – a comprehensive review, *IEEE Access*, vol. 8, pp. 144730–144766, 2020.

[53] A. A. Tavagnutti, D. Bosich, and G. Sulligoi, A multi-model methodology for stability assessment of complex DC microgrids, in *Proceedings of the 2021 IEEE Fourth International Conference on DC Microgrids (ICDCM)*, 2021, pp. 1–7.

[54] A. A. Tavagnutti, D. Bosich, and G. Sulligoi, Active damping poles repositioning for dc shipboard microgrids control, in *Proceedings of the 2021 IEEE Electric Ship Technologies Symposium (ESTS)*, 2021, pp. 1–8.

[55] L. Che and M. Shahidehpour, DC microgrids: economic operation and enhancement of resilience by hierarchical control, *IEEE Transactions on Smart Grid*, vol. 5, no. 5, pp. 2517–2526, 2014.

[56] F. Gao, R. Kang, J. Cao, and T. Yang, Primary and secondary control in DC microgrids: a review, *Journal of Modern Power Systems and Clean Energy*, vol. 7, no. 2, pp. 227–242, 2019.

[57] Y. Han, X. Ning, P. Yang, and L. Xu, Review of power sharing, voltage restoration and stabilization techniques in hierarchical controlled DC microgrids, *IEEE Access*, vol. 7, pp. 149202–149223, 2019.

[58] D. Bosich, G. Giadrossi, S. Pastore, and G. Sulligoi, Weighted bandwidth method for stability assessment of complex DC power systems on ships, *Energies*, vol. 15, p. 258, 2022.

[59] M. Amin and M. Molinas, Small-signal stability assessment of power electronics based power systems: a discussion of impedance- and eigenvalue-based methods, *IEEE Transactions on Industry Applications*, vol. 53, no. 5, pp. 5014–5030, 2017.

[60] G. O. Kalcon, G. P. Adam, O. Anaya-Lara, S. Lo, and K. Uhlen, Small signal stability analysis of multi-terminal VSC-based DC transmission systems, *IEEE Transactions on Power Systems*, vol. 27, no. 4 pp. 1818–1830, 2012.

[61] J. Beerten, S. DArco, and J. A. Suul, Identification and small-signal analysis of interaction modes in VSC MTDC systems, *IEEE Transactions on Power Delivery*, vol. 31, no. 2, pp. 888–897, 2016.

[62] L. Guo, S. Zhang, X. Li, Y. W. Li, C. Wang, and Y. Feng, Stability analysis and damping enhancement based on frequency-dependent virtual impedance for DC microgrids, *IEEE Journal of Emerging and elected Topics in Power Electronics*, vol. 5, no. 1, pp. 338–350, 2017.

[63] A. Maulik and D. Das, Stability constrained economic operation of islanded droop-controlled DC microgrids, *IEEE Transactions on Sustainable Energy*, vol. 10, no. 2, pp. 569–578, 2019.

[64] D. Bosich, M. Gibescu, and G. Sulligoi, Large-signal stability analysis of two power converters solutions for DC shipboard microgrid, in *Proceedings of the*

2017 IEEE Second International Conference on DC Microgrids (ICDCM), 2017, pp. 125–132.

[65] D. Bosich, A. Vicenzutti, and G. Sulligoi, Robust voltage control in large multi-converter MVDC power systems on ships using thyristor interface converters, in *Proceedings of the 2017 IEEE Electric Ship Technologies Symposium (ESTS)*, Arlington, VA, 2017, pp. 267–273.

[66] M. H Rashid, *Power Electronics Handbook: Devices, Circuits, and Applications*, Burlington, MA: Academic, 2006.

[67] N. Mohan, T. M. Undeland, and W. P. Robbins, *Power Electronics, Converters, Applications and Design*, New York, NY: John Wiley and Sons, Inc., 2003.